Single transverse mode protein laser

Itir Bakis Dogru, Kyungtaek Min, Muhammad Umar, Houman Bahmani Jalali, Efe Begar, Deniz Conkar, Elif Nur Firat Karalar, Sunghwan Kim, and Sedat Nizamoglu

Citation: Appl. Phys. Lett. **111**, 231103 (2017); doi: 10.1063/1.5007243

View online: https://doi.org/10.1063/1.5007243

View Table of Contents: http://aip.scitation.org/toc/apl/111/23

Published by the American Institute of Physics

Articles you may be interested in

Periodic pattern of liquid crystal molecular orientation induced by ultrasound vibrations
Applied Physics Letters **111**, 231101 (2017); 10.1063/1.5010213

Polariton condensation in S- and P-flatbands in a two-dimensional Lieb lattice
Applied Physics Letters **111**, 231102 (2017); 10.1063/1.4995385

Anti-reflective coating for visible light using a silver nanodisc metasurface with a refractive index of less than 1.0
Applied Physics Letters **111**, 231105 (2017); 10.1063/1.5000531

Optical side-band generation in THz Fabry-Perot laser cavities
Applied Physics Letters **111**, 231106 (2017); 10.1063/1.5001334

GaSb solar cells grown on GaAs via interfacial misfit arrays for use in the III-Sb multi-junction cell
Applied Physics Letters **111**, 231104 (2017); 10.1063/1.4991548

High-efficiency and low-loss gallium nitride dielectric metasurfaces for nanophotonics at visible wavelengths
Applied Physics Letters **111**, 221101 (2017); 10.1063/1.5007007



Reuse of AIP Publishing content is subject to the terms at: https://publishing.aip.org/authors/rights-and-permissions. Downloaded to: 88.255.99.40 on 14 November 2018, At: 01:43

Single transverse mode protein laser

Itir Bakis Dogru,[1,a)] Kyungtaek Min,[2,a)] Muhammad Umar,[2] Houman Bahmani Jalali,[1] Efe Begar,[3] Deniz Conkar,[3] Elif Nur Firat Karalar,[3] Sunghwan Kim,[2,4,b)] and Sedat Nizamoglu[1,5,b)]

[1]*Graduate School of Biomedical Sciences and Engineering, Koc University, Sariyer, Istanbul 34450, Turkey*
[2]*Department of Energy Systems Research, Ajou University, Suwon 16499, South Korea*
[3]*Department of Molecular Biology and Genetics, Koc University, Sariyer, Istanbul 34450, Turkey*
[4]*Department of Physics, Ajou University, Suwon 16499, South Korea*
[5]*Department of Electrical and Electronics Engineering, Koc University, Sariyer, Istanbul 34450, Turkey*

(Received 1 October 2017; accepted 15 November 2017; published online 5 December 2017)

Here, we report a single transverse mode distributed feedback (DFB) protein laser. The gain medium that is composed of enhanced green fluorescent protein in a silk fibroin matrix yields a waveguiding gain layer on a DFB resonator. The thin TiO_2 layer on the quartz grating improves optical feedback due to the increased effective refractive index. The protein laser shows a single transverse mode lasing at the wavelength of 520 nm with the threshold level of 92.1 $\mu J/mm^2$. *Published by AIP Publishing.* https://doi.org/10.1063/1.5007243

Biomaterials advantageously offer biocompatibility, biodegradability, genetic encoding, and eco-friendly processing to photonic technologies. A wide range of biomaterials show strong spontaneous emission, which is observed in riboflavin, chlorophyll, collagen, urine, and many others.[1] The use of the light-emitting biomaterials as optical gain media can open up a new direction for combining biomaterials and laser technology for sensing and light generation.[2–5]

In the last few decades, fluorescent proteins, first derived from luminescent jellyfish, initiated a new ground in biomedical researches, and today they are one of the most frequently used biomolecules in cell biology and biomedicine. Fluorescent proteins offer genetic variants that cover the emission bands in the entire visible region, high quantum yield, strong absorption cross section, and stability.[6] Therefore, fluorescent proteins are compelling materials for photonic applications. In addition, fibroin proteins, which are extracted from *Bombyx mori* (silkworm) silk, can be easily modified, their biodegradation time can be tuned, and they can be processed by both aqueous and organic solvents.[7] Beneficially, a silk fibroin protein solution can be poured on a surface to generate transparent films, which can enable its use as an optical material.[8] With these outstanding features, the silk fibroin has a widespread use in biophotonics, and so far, lenses, waveguides, fibers, and opals are fabricated from it.[9]

Recently, fluorescent protein usage took a step further, and they have been utilized as the gain medium in protein lasers. So far, enhanced green fluorescent proteins (eGFPs) have been used in living mammalian cells, *Escherichia coli* (*E. coli*), and the solid-state ring form for lasers.[5,10,11] Different from the previous cavity structures, distributed feedback (DFB) lasers show high wavelength selectivity by suppressing other bands.[12] Designing the lattice parameters and determining the substrate in terms of the refractive index (RI) result in mode control with a high beam quality. After the fabrication of the resonator, deposition of the gain medium is also an easy and fast step via casting or spin coating.[3,13] These unique properties of DFB lasers allow fabrication from a wide variety of materials.[14]

Here, we merge the advantageous properties of eGFP and silk fibroin to yield an all-protein gain medium. eGFP was doped in the silk protein matrix, and it was spin-coated on a distributed feedback (DFB) resonator made of TiO_2/quartz grating (see Fig. 1). In the plane of the DFB, the periodicity of the grating (Λ) was utilized as 330 nm to match the resonator modes to the optical gain spectrum. The laser emission was observed at the wavelength of 520 nm with a low threshold level of 92.1 $\mu J/mm^2$.

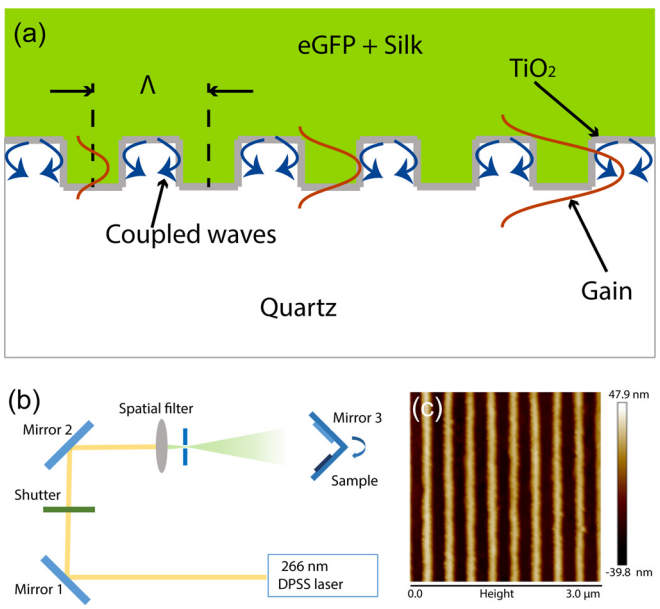


FIG. 1. (a) Schematic diagram of the single transverse mode protein DFB laser (not drawn in scale). (b) Schematic of the laser holography lithography (LHL) setup. The LHL setup mainly consists of a 266 nm diode-pumped solid-state source laser, a spatial filter, and a rotational stage. (c) AFM image of DFB quartz grating with a pitch size of 330 nm.

[a)]I. B. Dogru and K. Min contributed equally to this work.
[b)]Authors to whom correspondence should be addressed: sunghwankim@ajou.ac.kr and snizamoglu@ku.edu.tr

For the fabrication of the quartz grating, the template was fabricated on square-shaped quartz samples of $1 \times 1\,cm^2$. First, a 50 nm thick Cr layer was deposited on the cleaned quartz sample using an e-beam evaporator (ZZS550-2/D, Maestech). A negative photoresist (AZ nLOF 2070, Microchemicals) was then spin-coated on the Cr surface with the thickness of 250 nm by controlling the spin-coating speed to 4000 rpm, followed by post baking at 95 °C for 1 min. Further, the sample was subjected to laser beam interference to generate a 1D diffraction grating pattern by the laser holography lithography (LHL) method [Fig. 1(b)]. The LHL system mainly consists of a 266 nm diode-pumped solid-state source laser (FQCW266-50, CryLas), a spatial filter, and a Lloyd's mirror stage. The desired duty cycle and the grating period were controlled by the exposure time and the incident beam angle. The exposed sample was baked at 100 °C for 1 min, and then, the exposed resist was developed. The resist pattern was transferred to the underlying Cr-deposited quartz substrate using reactive-ion etching equipment (RIE 80 plus, Oxford Instrument). The quartz grating was obtained by the conventional Cl_2, CF_4-based RIE process, and the residual Cr layer was removed by wet-etching. Figure 1(c) shows the AFM image of the DFB grating with a grating period of 330 nm.

For eGFP solution preparation, GST-tag containing *Escherichia coli* (*E. coli*) cells are used. First, a tagged vector is transformed into *E. coli* cells, and cells are grown on plates. GST-tag (26 kDa), which is linked to the N terminal of eGFP (30 kDa) containing vector, is transformed into *E. coli* cells, and cells are grown on plates. After choosing a bacterial colony, large scale growth is started. eGFP expression is induced by the usage of 1 mM isopropyl β-d-1-thiogalactopyranoside. For the purification processes, bacteria are pelleted using centrifugal force, cells are lysed using lysozyme enzyme, and by freezing-thawing-sonication processes, purified protein is washed using GST Wash Buffer [1× PBS (phosphate-buffered saline), 0.25 M KCl, freshly supplied with 25 μg/ml leupeptin-pepstatin-chymostatin (LPC), 17.4 μg/ml phenylmethylsulfonyl fluoride (PMSF), and 10 μg/ml Aprotinin]. eGFP is purified by superflow glutathione agarose beads and eluted using the elution buffer (50 mM Tris pH 8.0, 10 mM Glutathione, freshly supplied with 10 mM dithiothreitol (DTT), and 25 μg/ml LPC) with centrifugal filters. Lastly, purified eGFP is concentrated using filters and 1× PBS (phosphate buffered saline) until it is concentrated down to 300 μl. Desalting is performed using dialysis membranes. At the end of the process, 7.96 mg/ml eGFP solution is obtained.

For silk fibroin solution preparation, *Bombyx Mori* silk cocoons were cut and separated from silkworms. 0.02 M aqueous Na_2CO_3 solution was prepared with boiled water, and 5 g of cocoon was added. This silk fibroin was rinsed and stirred with deionized water twice. Then, it was dried in air at room temperature. Dried silk fibroin was dissolved in 9.3 M LiBr solution. Following the 4 h heating process at 60 °C, the viscous silk solution was obtained. It was injected into a dialysis cassette, and this cassette was inserted in distilled water and stirred. This step was proceeded for 2 days changing the water at time intervals to remove LiBr and other contaminants. Lastly, the silk solution was taken from dialysis cassette and centrifuged at 9000 rpm at –2 °C for 20 min twice.[15] The final concentration of the silk fibroin solution was 7–9 wt. %.

Numerical simulations were performed using a commercial finite-difference time-domain (FDTD) software from Lumerical. Two-dimensional FDTD simulations were performed with the Bloch boundary condition ($k_x = 0$) in the x-direction, while the perfect matching layers were applied along the top and the bottom in the y-direction. The TiO_2 periodic surface was excited by setting multiple random poles to excite the periodic unit cell structure. Refractive index values of 1.54 (silk fibroin), 1.50 (quartz), and 2.45 (TiO_2) were used in the modelling. We obtained spectral and spatial data of the magnitude of the electric field by setting time conditions of 3000 fs.

A second order grating was employed in the fabricated DFB laser structure. The grating pitch size (Λ) of 330 nm was chosen to induce a second-order Bragg resonance wavelength ($\lambda_{Bragg} = \Lambda n_{eff}$, with n_{eff} being the effective refractive index of the waveguide mode) within the photoluminescence (PL) emission spectrum of the eGFP. Figures 2(a) and 2(b) show the simulated spectra and field profiles for the DFB structure made on a quartz substrate according to the designed parameters for the second order DFB laser with the pitch size of (Λ) of 330 nm, the grating depth of 65 nm, with 60% duty cycle, and the 200-nm thick gain layer. However, in this structure, the electric field is leaky to the quartz substrate due to the small index contrast between the quartz and the gain medium.

To achieve lasing, it is important to have sufficient optical gain in comparison with the optical losses. Therefore, it is critical to obtain a strong optical feedback by an optical resonator. In order to enhance field localization in the gain medium, a thin TiO_2 layer with a higher refractive index was deposited on the surface of the quartz grating. Applying a very thin TiO_2 layer to the silk/quartz interface induces a narrower field profile of the waveguide mode around the interface, and therefore, optical feedback and confinement are increased. The confinement factor of the electric field in the silk gain layer, defined in Eq. (1), [16] was almost doubled when the TiO_2 layer was applied, due to the increased n_{eff} [Fig. 3(a)]. Therefore, it is important to use a TiO_2 layer on quartz grating.

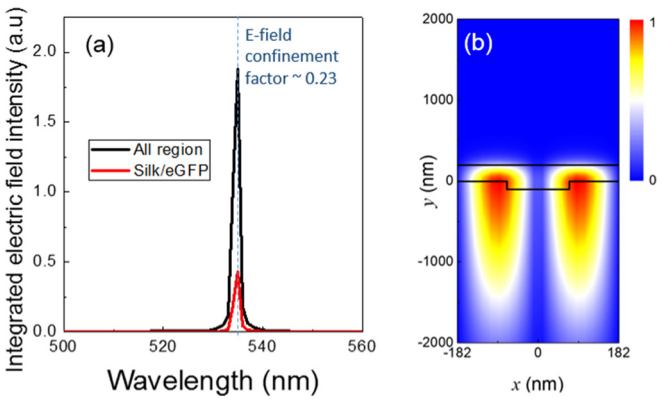


FIG. 2. (a) Spatially integrated electric field intensity in all the simulated region (black solid line) and in the optically active silk/eGFP film (red solid line) of the DFB structure. (b) The electric field profiles of resonance TE modes (l–534 nm).

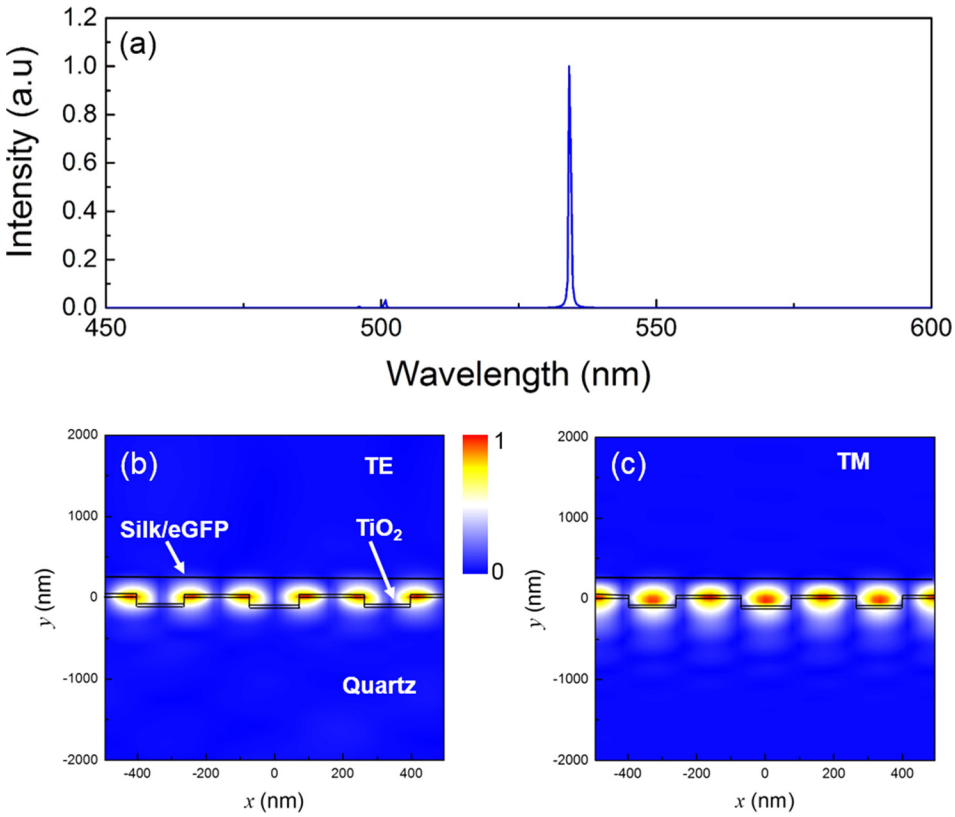


FIG. 3. (a) Simulation results for the 200 nm thick eGFP/silk fibroin gain layer with TiO_2 in the DFB structures. The simulated spectrum results show the resonance peaks. The normalized electric field profiles corresponding to the resonance mode at (b) 534.2 nm and (c) 500.8 nm.

The main peak at 534.2 nm, shown in Fig. 3(b), corresponds to TE polarization (with the magnetic field vertical, normal to the grating surface, and with the electric field parallel with the grating lines) and illustrates that the perturbation produced by the TiO_2 layer influences the coherent feedback provided by the grating structure. The TM resonance mode was investigated corresponding to the satellite peak at 500.2 nm in Fig. 3(c). The blue shifted resonance of the TM mode is due to a lower n_{eff} of the grating for the TM mode than for the TE mode, which is induced by different border conditions for TE and TM modes at the grating interfaces.

$$\text{Electric field confinement factor} = \frac{\int_{silk/eGFP} |E|^2 dA}{\int_{all\ region} |E|^2 dA}. \quad (1)$$

Here, eGFP shows a quasi-four level laser system as shown in Fig. 4(a), where the ground (S_0) state and the excitation state (S_1) include sub-energy levels.[5] In this laser system, the optical pump excites the molecule at S_0 to the S_1 that populates the molecule in the excited state.[17] Afterward, the molecule relaxes quickly to the lowest energy level in S_1, which is a long-lived state with a lifetime of about 1.7 ns (MicroTime 100, Picoquant) [see Fig. 4(b)]. Thus, at sufficiently high pumping levels, the transition between S_0 and S_1 levels results in population inversion and stimulated emission.

For population inversion, a Quanta-Ray INDI pulsed Nd:YAG laser is used with a typical pulse width of 7 ns and a repetition rate of 10 Hz. The excitation wavelength is adjusted as 483 nm by optical parametric oscillator (OPO) (Basiscan, SpectraPhysics) due to strong absorption of eGFP at this wavelength [see Fig. 4(c)]. The pump that is generated by the OPO passes through the optical density filter for laser transmission adjustment [Fig. 4(d)]. After the pump signal arrives to a 500 nm long pass dichroic filter, the dichroic filter reflects the pump laser and it passes through a cylindrical lens to have a line-shaped laser beam on the sample with the pump spot dimensions of 1 mm × 1 cm. Since the emitted light from the sample has a longer wavelength than 500 nm, it passes through

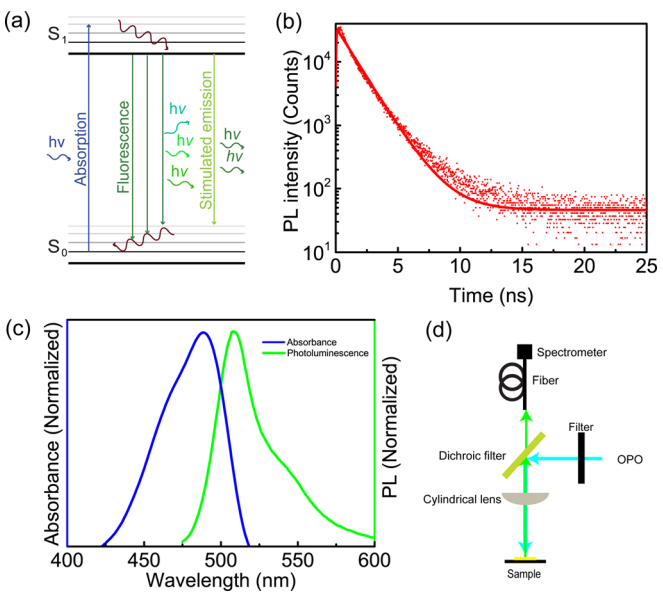


FIG. 4. (a) Quasi-four-level energy diagram of eGFP with absorption, fluorescence, and stimulated emission. (b) Time-resolved spectroscopy of 1:1 eGFP/silk at 520 nm that is spin-coated on glass. (c) Absorbance and photoluminescence spectrum of eGFP. (d) Schematic of the optical set-up for the laser emission measurement.

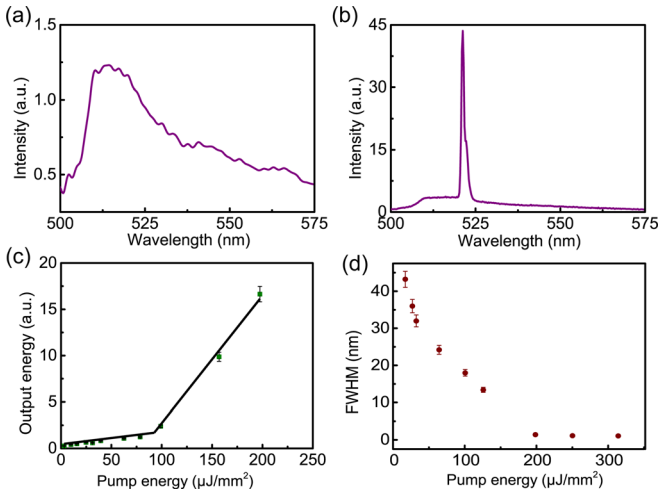


FIG. 5. Emission spectra of spin coated 1:1 eGFP solution/silk fibroin solution (a) below (b) and above threshold. (c) Measured light-light characteristic of the optically pumped DFB laser. (d) Full width at half maximum (FWHM) of emission as a function of pump flux.

the dichroic filter and reaches the spectrometer (Torus Concave Grating Spectrometer).

When the laser structure using the all-protein gain medium is optically pumped, initially a broad emission is observed due to the dominance of spontaneous emission of eGFP with respect to the stimulated emission at low pumping levels [see Fig. 5(a)]. Above 92.1 μJ/mm^2, a spectrally narrow peak starts to be observed [see Fig. 5(b)]. Moreover, the slope efficiency above the threshold increases 12 times in comparison to below the threshold [Fig. 5(c)]. While the FWHM was around 24 nm below the threshold, the FWHM reaches 1.1 nm above the threshold, which is close to the resolution of our spectrometer (ca. 1 nm) [Fig. 5(d)]. Furthermore, while the previous reports with fluorescent proteins present multi-mode laser emission due to the Fabry-Perot and whispering gallery resonators,[5,10,11] the distributed feedback cavity resulted in single transverse mode laser emission.

The threshold value of the protein laser is higher than the thresholds obtained from organic semiconductor DFB lasers and colloidal nanocrystal DFB lasers, which we attribute to the lower quantum yield of eGFP in the solid form and scattering-induced losses due to random packing of proteins.[11] The reduction of the threshold can decrease the adverse effect of laser light generation in cellular environments (e.g., bleb formation due to photothermal effects[18]). In comparison with conventional lasers, protein lasers are advantageous in terms of their biocompatibility that allows them to be interfaced with biological environments. In addition, their biodegradation time may be also programmed such that they can be safely absorbed by the living system after the laser finishes its function.[19] These lasers can be used for intracellular sensing and light-generation.[4,5,20]

In conclusion, eGFP in a silk fibroin protein matrix was employed as an optical gain material for a DFB laser with a second order grating fabricated on a quartz substrate with laser holography lithography. The laser holography lithography method was used to fabricate the large area grating that was designed according to absorption and emission spectra of eGFP. To provide a strong optical feedback, a biocompatible TiO_2 thin film was coated on the quartz grating. The spectral properties combined with the input-output energy relation reveal a single transverse mode protein laser. The biocompatibility of the laser holds promise for interfacing with biological cells or tissues that can be used for biosensing.

S.N. acknowledges the Turkish Academy of Sciences and the Scientific and Technological Research Council of Turkey (TUBITAK) with Project Nos. 114F317, 115E242, 115F451, and 114E194. SN acknowledges the support by Marie Curie Career Integration Grant (PROTEINLED, 631679). S.K. acknowledges support from the National Research Foundation (NRF) of Korea (No. 2017R1A2B4010807).

[1]M. Large, *Optical Biomimetics: Materials and Applications* (Elsevier, 2012).
[2]S. Nizamoglu, M. C. Gather, and S. H. Yun, Adv. Mater. **25**(41), 5943 (2013); X. Fan and S.-H. Yun, Nat. Methods **11**(2), 141 (2014).
[3]Y. Choi, H. Jeon, and S. Kim, Lab Chip **15**(3), 642 (2015).
[4]M. Humar and S. H. Yun, Nat. Photonics **9**, 572 (2015).
[5]M. C. Gather and S. H. Yun, Nat. Photonics **5**(7), 406 (2011).
[6]N. C. Shaner, P. A. Steinbach, and R. Y. Tsien, Nat. Methods **2**(12), 905 (2005).
[7]H. Perry, A. Gopinath, D. L. Kaplan, L. Dal Negro, and F. G. Omenetto, Adv. Mater. **20**(16), 3070 (2008); B. Kundu, R. Rajkhowa, S. C. Kundu, and X. G. Wang, Adv. Drug Delivery Rev. **65**(4), 457 (2013).
[8]H. Tao, D. L. Kaplan, and F. G. Omenetto, Adv. Mater. **24**(21), 2824 (2012).
[9]B. D. Lawrence, M. Cronin-Golomb, I. Georgakoudi, D. L. Kaplan, and F. G. Omenetto, Biomacromolecules **9**(4), 1214 (2008); S. T. Parker, P. Domachuk, J. Amsden, J. Bressner, J. A. Lewis, D. L. Kaplan, and F. G. Omenetto, Adv. Mater. **21**(23), 2411 (2009); S. Kujala, A. Mannila, L. Karvonen, K. Kieu, and Z. P. Sun, Sci. Rep. **6**, 22358 (2016); S. Kim, A. N. Mitropoulos, J. D. Spitzberg, H. Tao, D. L. Kaplan, and F. G. Omenetto, Nat. Photonics **6**(12), 818 (2012).
[10]C. P. Dietrich, A. Steude, L. Tropf, M. Schubert, N. M. Kronenberg, K. Ostermann, S. Hofling, and M. C. Gather, Sci. Adv. **2**(8), e1600666 (2016).
[11]B. H. Robinson, Sci. Total Environ. **408**(2), 183 (2009).
[12]C. Gourgon, J. Robadey, D. Martin, F. Filipowitz, L. Mahler, N. H. Ky, D. Deveaud, and F. K. Reinhart, IEEE Photonics Technol. Lett. **12**(7), 765 (2000).
[13]R. Xia, G. Heliotis, P. N. Stavrinou, and D. D. C. Bradley, Appl. Phys. Lett. **87**(3), 031104 (2005).
[14]J. Herrnsdorf, B. Guilhabert, Y. Chen, A. L. Kanibolotsky, A. R. Mackintosh, R. A. Pethrick, P. J. Skabara, E. Gu, N. Laurand, and M. D. Dawson, Opt. Express **18**(25), 25535 (2010); S. Riechel, U. Lemmer, J. Feldmann, T. Benstem, W. Kowalsky, U. Scherf, A. Gombert, and V. Wittwer, Appl. Phys. B: Lasers Opt. **71**(6), 897 (2000).
[15]D. N. Rockwood, R. C. Preda, T. Yucel, X. Q. Wang, M. L. Lovett, and D. L. Kaplan, Nat. Protoc. **6**(10), 1612 (2011).
[16]V. Passaro and M. La Notte, Sensors **12**(3), 2436 (2012).
[17]B. C. J. Zoeteman, H. R. Krikke, and J. Venselaar, Int. J. Adv. Manuf. Technol. **47**(5–8), 415 (2010).
[18]S. Nizamoglu, K.-B. Lee, M. C. Gather, K. S. Kim, M. Jeon, S. Kim, M. Humar, and S.-H. Yun, Adv. Opt. Mater. **3**, 1197 (2015).
[19]S. Nizamoglu, M. C. Gather, M. Humar, M. Choi, S. Kim, K. S. Kim, S. K. Hahn, G. Scarcelli, M. Randolph, and R. W. Redmond, Nat. Commun. **7**, 10374 (2016).
[20]M. C. Gather and S. H. Yun, Opt. Lett. **36**(16), 3299 (2011).